FRICTION AND THE INVERTED PENDULUM STABILIZATION PROBLEM

Sue Ann Campbell * Stephanie Crawford † Kirsten Morris‡

ABSTRACT

We consider an experimental system consisting of a pendulum, which is free to rotate 360 degrees, attached to a cart. The cart can move in one dimension. We study the effect of friction on the design and performance of feedback controllers that aim to stabilize the pendulum in the upright position. We show that a controller designed using a simple viscous friction model has poor performance - small amplitude oscillations occur when the controller is implemented. We consider various models for stick slip friction between the cart and the track and measure the friction parameters experimentally. We give strong evidence that stick slip friction is the source of the small amplitude oscillations. A controller designed using a stick slip friction model stabilizes the system, and eliminates the small amplitude oscillations. We show that a time delay in the feedback can lead to bistability.

Keywords: inverted pendulum, friction, feedback control, stability analysis.

1 Introduction

Although friction, which dissipates energy in a system, would seem to be a stabilizing force, it has been shown [1] that underestimating the size of the friction coefficient may sometimes lead to instability in a feedback control system. Friction has also been associated with oscillatory behaviour. Friction generated limit cycles were shown in simulations of a simple cart system [2] and were observed experimentally in a balancing apparatus in [3]. Oscillatory behaviour was predicted theoretically in a balancing system with backlash [4].

Here we examine the role of friction models in the design of a controller to balance a pendulum in the inverted position. In particular, we study the experimental system depicted schematically in Figure 1. In this system, a pendulum is attached to the side of a cart by means of a pivot which allows the pendulum to swing in the xy-plane. A force $F(t)$ is applied to the cart in the x direction, with the purpose of keeping the pendulum balanced upright.

Note that we focus here on stabilizing the pendulum in the upright position. This is in contrast to the swing-up problem, where one designs a controller to bring the pendulum close the upright pendulum and then employs a controller, such as we will discuss, to stabilize it. Details on the swing-up problem may be found in [5, 6].

The equations of motion of the cart and pendulum from Figure 1 can be found using Hamilton's Principle. They are:

$$\begin{aligned}(M+m)\ddot{x}(t) - ml\sin\theta(t)\dot{\theta}(t)^2 + ml\cos\theta(t)\ddot{\theta}(t) &= F(t) + F_{\text{fric}}(t),\\ ml\cos\theta(t)\ddot{x}(t) - mgl\sin\theta(t) + \tfrac{4}{3}ml^2\ddot{\theta}(t) &= 0,\end{aligned} \tag{1}$$

where x is the position of the cart, θ is the pendulum angle, measured in degrees away from the upright position, F is the force applied to the cart and F_{fric} is the force of friction. The definitions of the parameters and their values are given in Table 1.

In our experimental system, supplied by Quanser Limited, the applied force is due to a motor in the cart and is given by

$$F(t) = \alpha V(t) - \beta\dot{x}(t), \tag{2}$$

*Department of Applied Mathematics, University of Waterloo, Waterloo, ON N2L 3G1, Canada and Centre for Nonlinear Dynamics in Physiology and Medicine, McGill University, Montréal, QC H3A 2T5, Canada (sacampbell@uwaterloo.ca). Corresponding author.

†Department of Applied Mathematics, University of Waterloo, Waterloo, ON N2L 3G1, Canada (scrawford@alumni.uwaterloo.ca)

‡Department of Applied Mathematics, University of Waterloo, Waterloo, ON N2L 3G1, Canada (kmorris@uwaterloo.ca)

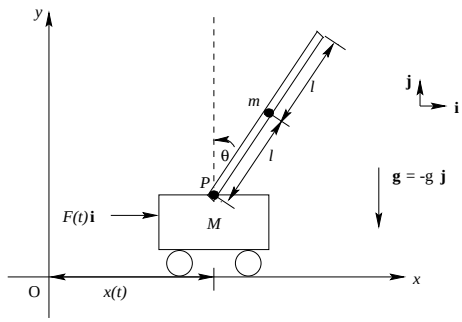

Figure 1. Inverted Pendulum System

Table 1. Parameter Values

Parameter	Description	Value
M	mass of the cart	0.8150 Kg
m	mass of the pendulum	0.210 Kg
l	distance from pivot to center of mass of the pendulum	0.3050 m
g	gravity constant	9.8 m/s
α	voltage to force conversion factor	1.7189
β	electrical resistance to force conversion factor	7.682

where V is the voltage supplied to the engine, and the second term represents electrical resistance in the cart. The values of the constants α and β for the motor used in our experimental apparatus are given in Table 1.

In [7], this system was studied assuming that the only kind of friction present was viscous friction, so that

$$F_{\text{fric}} = -\varepsilon \dot{x}, \tag{3}$$

where ε is the coefficient of viscous friction. With this assumption, if there is no applied force, $F(t) = 0$, and the system has a family of equilibrium points $(x, \theta, \dot{x}, \dot{\theta}) = (c, n\pi, 0, 0)$, where c is an arbitrary real number and n an arbitrary integer. The parameter c indicates that the final position of the cart varies, depending on the initial condition. There are two types of equilibria: n odd corresponds to the pendulum hanging straight down; n even corresponds to the pendulum pointing straight upward. We will refer to these as the down and up equilibria, respectively. It is well known (see e.g. [7]) that the down equilibrium point is stable and the up equilibrium point is unstable. In [7] a feedback controller was designed for this system, to balance the pendulum in the upright position. The controller was designed using an optimal linear quadratic controller (see e.g. [8]). Using stability analysis and numerical simulations, it was verified in [7] that for the model (1) with the friction law (3) the controlled system led to the upright position being a stable equilibrium point (dashed line in Figure 2). However, when the controller was implemented in the experimental system, small oscillations resulted (solid line in Figure 2(b)). By varying the design parameters, we were able to produce several different controllers which were theoretically stabilizing. All yielded the same oscillatory behaviour when implemented in the experimental system. This suggests that these oscillations are due to an inaccuracy in the model for the system used to design the controller.

It is the purpose of the current paper to investigate whether these oscillations were due to the friction model used and whether a more accurate friction law can be used to design a better controller. To this end, in the following section we introduce various friction models and estimate the model parameters experimentally. In section 3 we use linearization and numerical simulations to study the stability of the up equilibrium point of the controlled system using the new friction models. In section 4 we design a new controller using the new friction models and show that it achieves better results. In section 5 we study the effect of time delay in the controller. Finally, in section

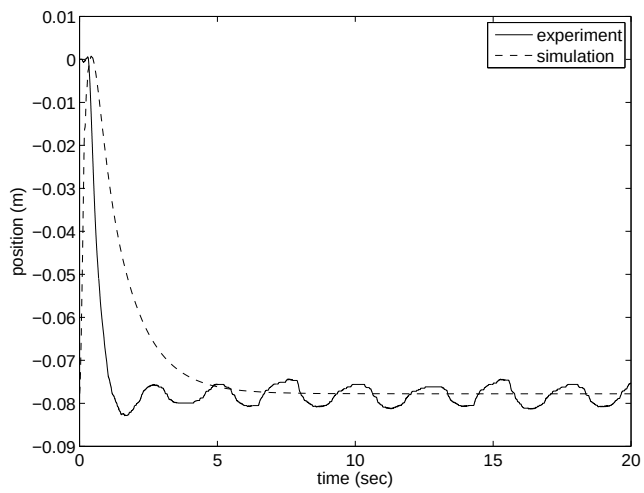

Figure 2. Experiment and simulation with simple viscous friction model.

6 we summarize our work and draw some conclusions.

2 Friction Models

A more accurate model of the friction between the cart and the track includes static and Coulomb (sliding) friction as well as viscous friction. Static friction is the friction that must be overcome to start an object moving; it is only present when the object is not moving. Coulomb and viscous friction are both present only when the object is moving. Thus, the simplest model incorporating all these effects is:

$$F_{\text{fric}} = \begin{cases} F_{\text{static}} & \text{if } \dot{x} = 0, \\ F_{\text{coulomb}} + F_{\text{viscous}} & \text{if } \dot{x} \neq 0. \end{cases} \tag{4}$$

The various components have well known models:

$$F_{\text{static}} = \begin{cases} -F_{\text{applied}} & \text{if } |F_{\text{applied}}| < \mu_s F_N \\ -\mu_s F_N \operatorname{sgn}(F_{\text{applied}}) & \text{if } |F_{\text{applied}}| \geq \mu_s F_N \end{cases}, \tag{5}$$

$$F_{\text{coulomb}} = -\mu_c F_N \operatorname{sgn}(\dot{x}), \tag{6}$$

$$F_{\text{viscous}} = -\varepsilon \dot{x}, \tag{7}$$

where μ_s, μ_c, ε are the coefficients of static, Coulomb and viscous friction, respectively, and F_N is the magnitude of the normal force. In our model, the object is moving horizontally, so $F_N = (m+M)g$. The values of the various parameters were estimated experimentally, as outlined in Appendix A. These values are listed in Table 2.

2.1 Exponential Friction Model

To test the friction model we used the following experiment. The pendulum was detached from the cart and then the voltage in the cart motor (and hence the applied force to the cart) was slowly ramped up. Figure 3 shows a comparison between the data from once such

Table 2. Parameters for Simple Friction Model

Parameter	Description	Experimental Estimate
μ_s	coefficient of static friction	0.08328
μ_c	coefficient of Coulomb friction	0.04287
ε	coefficient of viscous friction	2.3156

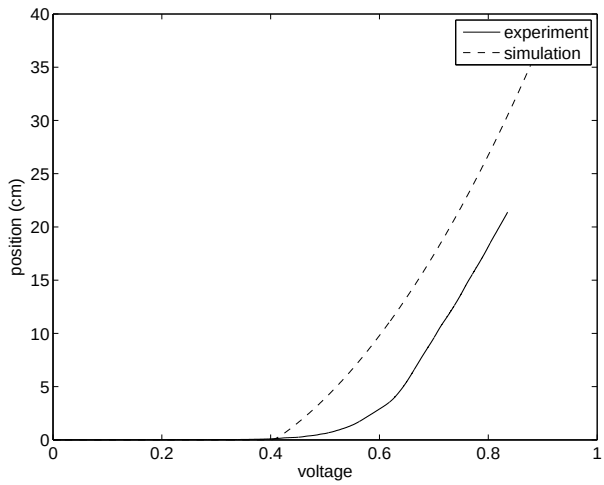

Figure 3. Comparison of voltage ramp experiment and simulation using the simple friction model (4). Parameters are given in Tables 1 and 2.

experiment and a simulation of the corresponding model for the cart (33) with the friction model (4)–(7) and the parameters given in Tables 1 and 2. It is clear that the simulated data do not entirely fit the experimental data. In particular, the transition from the cart being stationary to it moving is smoother in the experiment than in the simulation. Hauschild [9] has suggested adding an exponential factor to smooth this transition. The model for the friction between the cart and the track then becomes:

$$F_{\text{fric}} = \begin{cases} F_{\text{static}} & \text{if } \dot{x} = 0, \\ -(\mu_c + (\mu_s - \mu_c)e^{-(\frac{\dot{x}}{v_s})^{\gamma}})F_N \operatorname{sgn}(\dot{x}) - \varepsilon\dot{x} & \text{if } \dot{x} \neq 0, \end{cases} \tag{8}$$

where F_N is as defined above, v_s is called the Stribeck velocity and γ the form factor. To fit the new parameters, we plotted the simulations with the exponential friction model together with the experimental data, and adjusted the parameters v_s and γ to fit the data. The values so chosen are:

$$\gamma = 2\,,\, v_s = 0.105. \tag{9}$$

Figure 4 shows the output of several experiments together with corresponding simulations of the model (33) with the exponential friction model (8) and parameters given by Tables 1, 2 and equation (9). The exponential friction model provides a much better approximation of the experimental data than the simple model. However, since the data does not fit that well for smaller velocities, it was decided to adjust the value of the coefficients of static and viscous friction. By fitting the data, it was determined that $\mu_s = 0.08610$ and $\varepsilon = 3$ give better results for smaller velocities while not sacrificing the results for larger velocities (see Figure 5). These values, summarized in Table 3, will be used for the remainder of the paper.

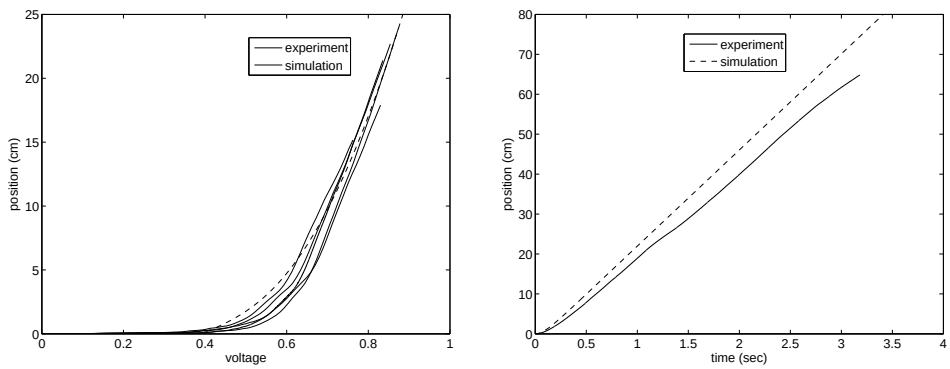

(a) Voltage ramp

(b) Constant applied voltage of 1.6 volts

Figure 4. Experiments vs simulations using exponential friction model with $\mu_s = 0.08328, \mu_c = 0.04287, \varepsilon = 2.3156, v_s = 0.105, \gamma = 2$.

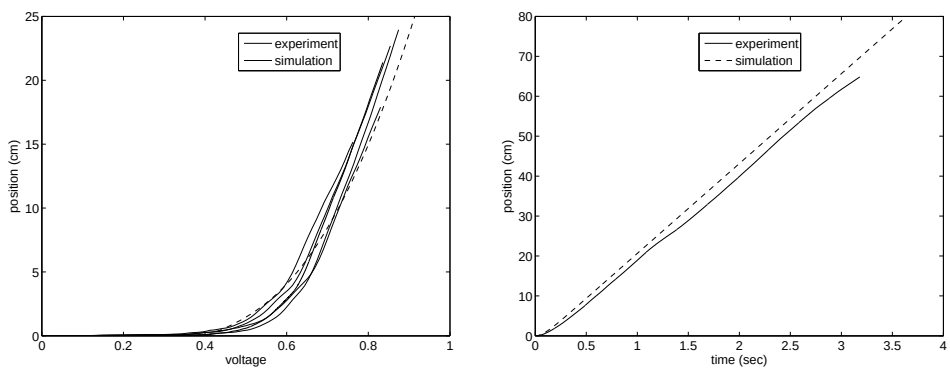

(a) Voltage ramp

(b) Constant Voltage = 1.6

Figure 5. Experiments vs simulations using exponential friction model with $\mu_s = 0.08610, \mu_c = 0.04287, \varepsilon = 3, v_s = 0.105, \gamma = 2$.

2.2 Dynamic Friction Model

The exponential friction model studied in the last section fits the experimental data reasonably well, however, for comparison we consider an alternative model, due to Canudas de Wit and Lipschinksy [10]. This model attempts to represent friction more physically by thinking of two surfaces making contact through elastic bristles. The main idea is that when a force is applied, the bristles will deflect like springs, which gives rise to the friction force. The friction force generated by the bristles is

$$F_{\text{fric}} = -\sigma_0 z - \sigma_1 \frac{dz}{dt} - \varepsilon \dot{x},$$

where z is the average deflection of the bristles, and σ_0, σ_1 are the stiffness and damping coefficient. The variation of z is modelled via:

$$\frac{dz}{dt} = \dot{x} - \sigma_0 \frac{|\dot{x}|}{g(\dot{x})} z \tag{10}$$

Table 3. Parameters for Exponential Friction Model

Parameter	Description	Value
μ_s	coefficient of static friction	0.08610
μ_c	coefficient of Coulomb friction	0.04287
ε	coefficient of viscous friction	3
v_s	Stribeck velocity	0.105
γ	form factor	2

where

$$g(\dot{x}) = (\mu_c + (\mu_s - \mu_c)e^{-(\frac{\dot{x}}{v_s})^\gamma})F_N.$$

This leads to a dynamic friction force

$$F_{\text{fric}} = -(\sigma_1 + \varepsilon)\dot{x} - \sigma_0 z\left(1 - \sigma_1 \frac{|\dot{x}|}{g(\dot{x})}\right), \tag{11}$$

where z satisfies (10).

Note that when $\dot{x}$ is constant, the bristle state z, and hence F_{fric}, approach constant values:

$$\begin{aligned} z &= \frac{1}{\sigma_0} g(\dot{x})\,\text{sgn}(\dot{x}), \\ F_{\text{fric}} &= -g(\dot{x})\,\text{sgn}(\dot{x}) - \varepsilon\dot{x} \\ &= -(\mu_c + (\mu_s - \mu_c)e^{-(\frac{\dot{x}}{v_s})^\gamma})F_N\,\text{sgn}(\dot{x}) - \varepsilon\dot{x}. \end{aligned}$$

Thus, the steady state friction force is the same as that of the exponential friction model (8).

Since we have already determined the parameters for the exponential friction model (Table 3), we only need to determine σ_0 and σ_1. To obtain these parameters, we started out with values similar to those found in [9] and then adjusted them to fit the experimental data. The values we found for the parameters are given in Table 4. Figure 6 shows experimental results together with simulations of the model

Table 4. Parameters for Dynamic Friction Model

Parameter	Description	Value
σ_0	stiffness	121
σ_1	damping coefficient	70

(33) using the dynamic friction model (11) with parameters as in Tables 1,3 and 4. Comparing with Figure 5 we see that both friction models fit the data quite well.

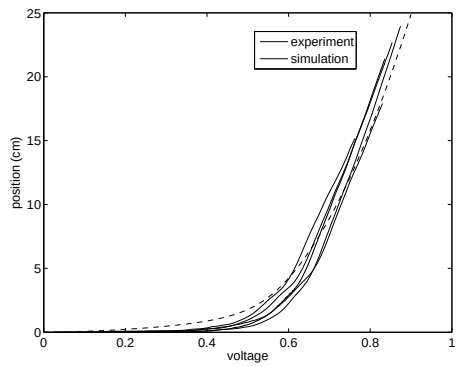

Figure 6. Experiment vs simulation using dynamic friction model with σ_0=121 and σ_1=70. Other parameters are as in Figure 5.

3 New Friction Models with Old Controller

In this section, we consider how the controller based on the viscous friction model affects the system with stick slip friction. We begin by reviewing how the controller is designed and give the controller based on the viscous friction model. We will then study the model for the full cart-pendulum system (1) with this controller and either the exponential or dynamic friction model. We will examine the linearized stability of the upright equilibrium point and show numerical simulations of the full nonlinear model.

Define the state

$$\mathbf{x}(\mathbf{t}) = (x_1(t), x_2(t), x_3(t), x_4(t))^T = (x(t), \theta(t), \dot{x}(t), \dot{\theta}(t))^T.$$

System (1) with applied force given by (2) and either of the friction models, can be written in first-order form and linearized to obtain an equation of the form

$$\dot{\mathbf{x}} = A\mathbf{x} + BV(t), \tag{12}$$

where $V(t)$ is the applied voltage and A and B depend on the model used for friction in the physical system.

To determine how to choose $V(t)$ to stabilize the up equilibrium point, we solve a linear quadratic control problem as described in, for example, [8]. In particular, we use the linear quadratic cost functional

$$\inf_{V(t)\in L_2(0,\infty)} \int_0^\infty \left[\mathbf{x}(t)^T Q\mathbf{x}(t) + rV(t)^2\right] dt,$$

where the weights $Q \geq 0$ and $r > 0$ are chosen to reflect the relative importance of reducing the states $\mathbf{x}$ and the cost of the control V. The solution to this problem is the feedback law

$$V(t) = K \cdot \mathbf{x}(t), \tag{13}$$

where the gain K depends on the choice of the design parameters r, Q and (through A and B) on the choice of friction model.

Since our system is linear and single-input, the control weight r can be absorbed into the state weight Q and was set to 1. The state weight Q is chosen to penalize the positions heavily with small costs on the velocities. This choice of weights penalizes non-zero position so that the resulting controller will maintain the pendulum near the upright position. Reducing the velocities to zero is a secondary objective. This reasoning led to $Q = \text{diag}(5000, 3000, 20, 20)$ in [7]. We shall use this same Q throughout the paper.

With the feedback controller (13) the applied force in (1) becomes

$$\begin{aligned} F(t) &= \alpha K \cdot (x, \theta, \dot{x}, \dot{\theta})^T - \beta \dot{x} \\ &= d_1 x + d_2 \theta + d_3 \dot{x} + d_4 \dot{\theta} - \beta \dot{x} \\ &\stackrel{def}{=} F_{\text{control}}. \end{aligned} \tag{14}$$

Note that when no control is applied, $F_{\text{control}} = 0$.

In [7] they consider system (1) with a simple simple viscous friction model $F_{fric} = \varepsilon \dot{x}$ ($\varepsilon = 2.1$). With Q as above they obtain the feedback gain

$$K = [k_1, k_2, k_3, k_4] = [70.7107, 142.5409, 50.6911, 26.9817]. \tag{15}$$

They then show that the up equilibrium is unstable if no control is applied ($F(t) = 0$) and locally stable if the controller (15) is used. In the following we study (1) with this controller, but with the more accurate stick slip friction models.

3.1 Exponential Model

In order to study the stability of the equilibrium points, we first transform the equation (1) into first-order form. Solving (1) for $\ddot{x}$ and $\ddot{\theta}$ yields a first order model:

$$\dot{\mathbf{x}} = \mathbf{f}(\mathbf{x}), \tag{16}$$

with

$$\mathbf{f}(\mathbf{x}) = \begin{pmatrix} x_3 \\ x_4 \\ \dfrac{F_{\text{control}} + F_{\text{fric}} + ml \sin x_2 x_4^2 - \frac{3}{4} mg \cos x_2 \sin x_2}{(M + m - \frac{3}{4} m (\cos x_2)^2)} \\ \dfrac{(-F_{\text{control}} - F_{\text{fric}}) \cos x_2 - ml \sin x_2 \cos x_2 x_4^2 + (M+m) g \sin x_2}{(\frac{4}{3} l)(M + m - \frac{3}{4} m (\cos x_2)^2)} \end{pmatrix},$$

where

$$F_{\text{control}} = d_1 x_1 + d_2 x_2 + d_3 x_3 + d_4 x_4 - \beta x_3, \tag{17}$$

$$F_{\text{fric}} = \begin{cases} F_{\text{static}} & \text{if } x_3 = 0 \\ -(\mu_c + (\mu_s - \mu_c) e^{-(\frac{x_3}{v_s})^\gamma}) F_N \operatorname{sgn}(x_3) - \varepsilon x_3 & \text{if } x_3 \neq 0 \end{cases}$$

and F_{static} is given by (5).

Let $\overline{\mathbf{x}}$ be an equilibrium point of (16). The linear (local) stability of $\overline{\mathbf{x}}$ is determined by the eigenvalues of the Jacobian of $\mathbf{f}$ evaluated at $\overline{\mathbf{x}}$, $D\mathbf{f}(\overline{\mathbf{x}})$. This requires that $\mathbf{f}$ be differentiable, thus an approximation of $\tanh(\delta \dot{x})$, with δ large, was used for $\operatorname{sgn}(\dot{x})$.

The equilibrium points satisfy $\mathbf{f}(\overline{\mathbf{x}}) = 0$, thus, as in [7], when no control is applied they are

$$\overline{\mathbf{x}} = (c, n\pi, 0, 0)^T,$$

where n in an integer and c is an arbitrary real number.

When control is applied, the equilibria are:

$$\bar{\mathbf{x}} = \left(\frac{-d_2}{d_1} n\pi, n\pi, 0, 0 \right)^T, \tag{18}$$

where d_1, d_2 are defined in (14). As before, the equilibria with n odd are the down equilibria and those with n even are the up equilibria. A simple calculation shows that with no control, the former are stable and the latter unstable.

We now analyze the stability of the system with the feedback control (14). With control, the Jacobian matrix of the linearization about the equilibria is

$$\begin{pmatrix} 0 & 0 & 1 & 0 \\ 0 & 0 & 0 & 1 \\ \frac{4d_1}{4M+m} & \frac{4d_2-3mg}{4M+m} & \frac{4(d_3-\beta-\varepsilon-\delta\mu_s(M+m)g)}{4M+m} & \frac{4d_4}{4M+m} \\ \frac{(-1)^{n+1}3d_1}{(4M+m)l} & \frac{(-1)^{n+1}3(d_2-(M+m)g)}{(4M+m)l} & \frac{(-1)^{n+1}3(d_3-\beta-\varepsilon-\delta\mu_s(M+m)g)}{(4M+m)l} & \frac{(-1)^{n+1}3d_4}{(4M+m)l} \end{pmatrix}$$

It follows that the characteristic equation for the Jacobian evaluated at the up equilibrium is

$$\lambda^4 + a_3\lambda^3 + a_2\lambda^2 + a_1\lambda + a_0 = 0, \tag{19}$$

where

$$\begin{aligned} a_3 &= \frac{3d_4 + 4l(\beta + \varepsilon + \delta\mu_s(M+m)g - d_3)}{(4M+m)l} \\ a_2 &= \frac{-3(M+m)g + 3d_2 - 4ld_1}{(4M+m)l} \\ a_1 &= \frac{-3g(\beta + \varepsilon + \delta\mu_s(M+m)g - d_3)}{(4M+m)l} \\ a_0 &= \frac{3d_1 g}{(4M+m)l}. \end{aligned}$$

Use of the Routh Hurwitz Criterion (e.g. [8]) shows that, for the parameter values of our experiment (Tables 1 and 3) and the control gain (15), this equation has two eigenvalues with positive real parts if $\delta > 60.4$. Since δ is large, this indicates that the up equilibrium is *unstable* for the system with the exponential friction model and the feedback control designed using the viscous friction model. This agrees with the fact that the physical system did not settle into the equilibrium point. Further, for $60.4 < \delta \leq 241$, the eigenvalues with positive real parts occur in complex conjugates, which is consistent with the observation of oscillations in the physical system.

Numerical simulations of the full nonlinear system (1) with the exponential friction model (8), applied force (14) and the old controller (15) agree with the prediction of the linear analysis that the equilibrium point is unstable. Simulations which start close to the equilibrium point tend away from it and ultimately oscillate with constant amplitude. An example is shown in Figure 7, along with a typical experimental time trace. The simulation and the experiment exhibit oscillations with similar amplitude and frequency. (In Figure 7 and subsequent similar figures, the simulations have been shifted to overlap the experimental results, since the final position of the cart is arbitrary.)

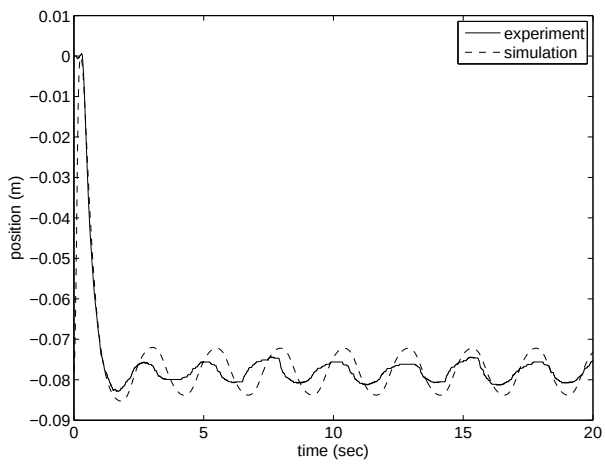

Figure 7. Comparison of experiment with controller (15) and simulation of pendulum cart system (1) with the same controller and the exponential friction model.

3.2 Dynamic Model

To obtain a first order model of the form (16), we need to use a five-dimensional state vector:

$$\mathbf{x} = (x_1, x_2, x_3, x_4, x_5)^T = (x, \theta, \dot{x}, \dot{\theta}, z).$$

This yields the first-order system

$$\dot{\mathbf{x}} = \begin{pmatrix} x_3 \\ x_4 \\ \dfrac{F_{\text{control}} + F_{\text{fric}} + ml\sin(x_2)x_4^2 - \frac{3}{4}mg\cos(x_2)\sin(x_2)}{M + m - \frac{3}{4}m(\cos(x_2))^2} \\ \dfrac{-\cos(x_2)(F_{\text{control}} + F_{\text{fric}}) + (M+m)g\sin(x_2) - ml\sin(x_2)\cos(x_2)x_4^2}{(\frac{4}{3}l)(M + m - \frac{3}{4}m(\cos(x_2))^2)} \\ x_3 - \dfrac{\sigma_0|x_3|x_5}{(\mu_c + (\mu_s - \mu_c)e^{(-(\frac{x_3}{v_s})^2)})F_N} \end{pmatrix},$$

where

$$F_{\text{fric}} = -(\sigma_1 + \varepsilon)x_3 - \sigma_0 x_5 \left(1 - \sigma_1 \frac{|x_3|}{g(x_3)}\right).$$

and F_{control} is given by (17).

When no control is applied, the equilibrium points are

$$\overline{\mathbf{x}} = (c, n\pi, 0, 0, h)^T,$$

where c, h are arbitrary real numbers and n is an arbitrary integer. When control is applied, the equilibrium points are

$$\overline{\mathbf{x}} = (\frac{-d_2}{d_1}n\pi, n\pi, 0, 0, h), \tag{20}$$

where d_1, d_2 are defined in (14). Once again, the equilibria with n odd are the down equilibria and those with n even are the up equilibria. A standard calculation shows that with no control, the former are stable and the latter unstable.

To calculate the Jacobian, $D\mathbf{f}(\overline{\mathbf{x}})$ requires that $\mathbf{f}$ be differentiable, so we must approximate $|x_3|$ by a differentiable function. Note that any such approximation will have derivative 0 when x_3 is 0, so the terms involving $|x_3|$ contribute nothing to the linearization. With control, then, the Jacobian matrix evaluated about the up equilibrium is

$$\begin{pmatrix} 0 & 0 & 1 & 0 & 0 \\ 0 & 0 & 0 & 1 & 0 \\ \frac{4d_1}{4M+m} & \frac{4d_2-3mg}{4M+m} & \frac{4(d_3-\beta-\sigma_1-\varepsilon)}{4M+m} & \frac{4d_4}{4M+m} & \frac{-4\sigma_0}{4M+m} \\ \frac{-3d_1}{(4M+m)l} & \frac{-3(d_2-(M+m)g)}{(4M+m)l} & \frac{-3(d_3-\beta-\sigma_1-\varepsilon)}{(4M+m)l} & \frac{-3d_4}{(4M+m)l} & \frac{(-1)^n 3\sigma_0}{(4M+m)l} \\ 0 & 0 & 1 & 0 & 0 \end{pmatrix}.$$

It follows that the characteristic equation for the Jacobian evaluated at the up equilibrium is

$$\lambda(\lambda^4 + a_3\lambda^3 + a_2\lambda^2 + a_1\lambda + a_0) = 0, \tag{21}$$

where

$$\begin{aligned} a_3 &= \frac{3d_4 + 4l(\beta+\varepsilon+\sigma_1-d_3)}{(4M+m)l} \\ a_2 &= \frac{4l\sigma_0 - 3(M+m)g + 3d_2 - 4ld_1}{(4M+m)l} \\ a_1 &= \frac{-3g(\beta+\varepsilon+\sigma_1-d_3)}{(4M+m)l} \\ a_0 &= \frac{3(d_1-\sigma_0)g}{(4M+m)l}. \end{aligned}$$

Note that there is always one zero eigenvalue. This is because the equilibrium points are not isolated but come in lines, since the z coordinate may take any value (see equation (20)). Using the parameter values of Tables 1, 3 and 4, the other four eigenvalues were found to be:

$$-118.4231342, -5.326811579, -0.1396838407 \pm 0.06683092600i$$

Since all the eigenvalues other than zero have negative real parts, the line of equilibrium points is *orbitally asymptotically stable*. This means that any initial condition close enough to the line will approach one of the points on the line [11, Theorem 4.3].

A numerical simulation of the full nonlinear system (1) with the dynamic friction model (11), the applied force (14) and the controller (15) is shown in Figure 8(a) along with the results of a typical experiment using the same controller. The simulation agrees with the experiment in that they both show oscillations, however, the frequency and amplitude match is not as good as with the exponential friction model. This simulation result seems to differ from the prediction from the linear stability analysis that the equilibrium point is stable. However, this is clarified by the simulations shown in Figure 8(b). In this case, two initial conditions very close to zero are chosen and one can see that the smaller one goes asymptotically to an equilibrium point while the larger one goes the periodic solution. Thus it would appear that with the dynamic friction model the equilibrium point is stable and coexists with a stable periodic orbit. Further, the basin of attraction of the equilibrium point is quite small, so most initial conditions lead to oscillations.

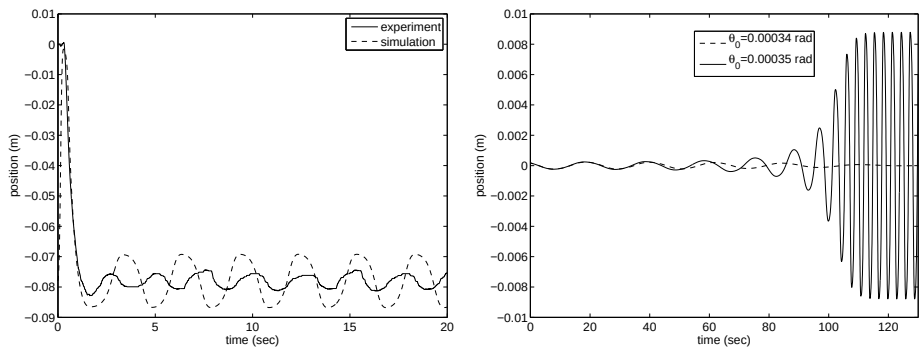

(a) (b)

Figure 8. Simulations of pendulum cart system (1) with the dynamic friction model (11) and the controller (15). (a) Initial angle is chosen for comparison with experiment. (b) Two initial angles very close to zero are chosen to illustrate the bistability between the equilibrium point and the periodic solution.

4 New Controllers for the New Friction Models

In this section we will use the exponential and dynamic friction models to design controllers to stabilize the upright equilibrium point. We use the same approach as the last section. The system (1) with applied force given by (2) and either of the friction models is written in first-order form and linearized to obtain equations of the form

$$\dot{\mathbf{x}} = A\mathbf{x} + BV(t) \tag{22}$$

where $V(t)$ is the applied voltage and A and B depend on the model (exponential or dynamic) used for friction in the physical system. To determine how to choose $V(t)$ to stabilize the up equilibrium point, we solve a linear quadratic control problem as described in the previous section.

4.1 Controller for the Exponential Model

In this case, the state is $\mathbf{x} = (x, \theta, \dot{x}, \dot{\theta})$. The matrices A and B are found by rewriting system (1), with $F(t) = 0$ and F_{fric} given by (8), as a four-dimensional first- order system and then linearizing about the upright equilibrium point. This yields

$$A = \begin{pmatrix} 0 & 0 & 1 & 0 \\ 0 & 0 & 0 & 1 \\ 0 & \frac{-3mg}{4M+m} & \frac{-4(\beta+\varepsilon+100F_s)}{4M+m} & 0 \\ 0 & \frac{3(M+m)g}{(4M+m)l} & \frac{3(\beta+\varepsilon+100F_s)}{(4M+m)l} & 0 \end{pmatrix},$$

$$B = \begin{pmatrix} 0 \\ 0 \\ \frac{4\alpha}{4M+m} \\ \frac{-3\alpha}{(4M+m)l} \end{pmatrix}.$$

We design the controller as discussed in the previous section and find the new feedback gain is:

$$K = [70.7107, 304.9273, 143.3152, 61.0833]. \tag{23}$$

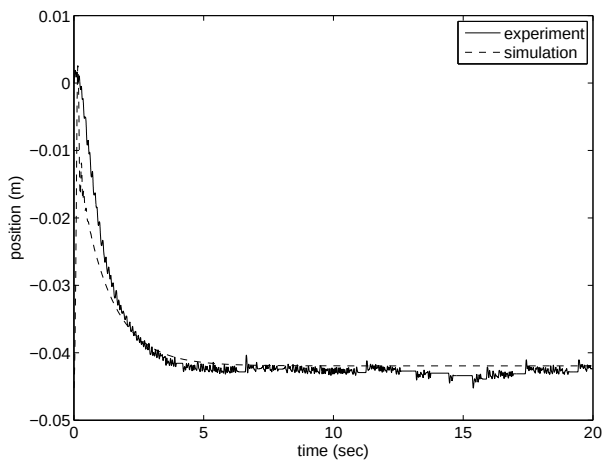

Figure 9. Implementation of the controller based on the exponential friction model in the experiment (solid line) and in a numerical simulation of the system with initial condition $(x, \theta, \dot{x}, \dot{\theta}) = (0, 0.06\,\text{rad}, 0, 0)$ (dashed line).

Numerical simulations of the full system (1) with the exponential friction model (8) confirm that the pendulum is stabilized in the inverted position by this controller. See Figure 9 for an example.

We implemented this controller in our experimental system and found that it did stabilize the system. An example experimental run is shown in Figure 9. The performance of the controlled system is considerably better than that obtained with the controller designed using the simple viscous friction model. Note that there remains some noise in the system. This will be discussed further in section 6.

4.2 Controller for the Dynamic Model

Here $\mathbf{x} = (x, \theta, \dot{x}, \dot{\theta}, z)$. The matrix A is found by rewriting system (1), with $F(t) = 0$ and F_{fric} given by (11), as a five dimensional first order system and then linearizing about the upright equilibrium. We obtain

$$A = \begin{pmatrix} 0 & 0 & 1 & 0 & 0 \\ 0 & 0 & 0 & 1 & 0 \\ 0 & \frac{-3mg}{4M+m} & \frac{-4(\beta+\sigma_1+\varepsilon)}{4M+m} & 0 & \frac{-4\sigma_0}{4M+m} \\ 0 & \frac{3(M+m)g}{(4M+m)l} & \frac{3(\beta+\sigma_1+\varepsilon)}{(4M+m)l} & 0 & \frac{3\sigma_0}{(4M+m)l} \\ 0 & 0 & 1 & 0 & 0 \end{pmatrix}.$$

B is the same as for the exponential friction model, except that we add a zero at the end, since the control signal is unaffected by the change in the friction model:

$$B = \begin{pmatrix} 0 \\ 0 \\ \frac{4\alpha}{4M+m} \\ \frac{-3\alpha}{(4M+m)l} \\ 0 \end{pmatrix}.$$

Ideally, a control system should be *controllable*. For our system this means, roughly, that there exists a control signal $V(t)$ to control the system from any initial state to any final state. *Stabilizability* is a weaker property. System (22) is stabilizable if there exists some matrix K such that $A - BK$ has all eigenvalues with negative real parts. A stabilizable system can be controlled from any initial state to zero.

The linear quadratic control problem can only be solved if the system is stabilizable. (See e.g. [8].) For system (22) to be stabilizable, the rank of

$$[(\lambda I - A) \;\; B]$$

for any positive or zero eigenvalue λ of A must be 5 [8]. It is easily checked that this system is not stabilizable. This is due to the introduction of the additional "friction state" z. The model must undergo a transformation so that it becomes controllable and stabilizable. The new model is given by:

$$\begin{aligned} \dot{\mathbf{s}} &= (UAU^{-1})\mathbf{s} + (UB)\mathbf{u} \\ &= \begin{bmatrix} A_c & A_{cu} \\ A_u & 0 \end{bmatrix} \begin{bmatrix} \mathbf{s}_c \\ \mathbf{s}_u \end{bmatrix} + \begin{bmatrix} B_c \\ 0 \end{bmatrix} V(t) \end{aligned} \tag{24}$$

where $\mathbf{s} = U\mathbf{x}$, and U is the transformation matrix. The subsystem

$$\dot{\mathbf{s}}_c(t) = A_c\mathbf{s}_c(t) + B_c V(t)$$

is controllable. We used the Matlab function `minreal`, to obtain a controllable subsystem of order 4. We now calculate the controller for the controllable subsystem, using the control weight $r = 1$ and transforming the state weight to $Q' = UQU^{-1}$ where Q is as for the other models. We obtain

$$K' = [136.0180, -124.0216, -58.1005, 288.9371].$$

This K' stabilizes the controllable subsystem. The feedback K for the original system is $K = K'U$. Thus the new K is:

$$K = [85.0828, 290.4957, 136.0180, 58.1005, 0]. \tag{25}$$

Putting $d_j = \alpha k_j$ in the characteristic equation (21) shows that the eigenvalues in this case are now:

$$0, -92.38161062, -9.394053324, -4.632006064, -0.1744814929.$$

The zero eigenvalue is due to the state z which cannot be controlled by the control signal. According to linear analysis, the up equilibrium point is orbitally asymptotically stable. This is confirmed by numerical simulations of the full system (1) with the exponential friction model (11). See Figure 10 for an example.

We implemented this controller in our experimental system and found that it did stabilize the system. An example experimental run is shown in Figure 10. Again, the performance is considerably better than that of the controlled system obtained using the simple viscous friction model. Note that, as with the controller based on the exponential friction model, there remains some noise in the system. This will be discussed further in section 6.

5 Effect of Time Delay

As illustrated in the last section, the controller designed with either friction model achieves stability of the upright equilibrium point. We would now like to compare their robustness with respect to time delay in the feedback loop.

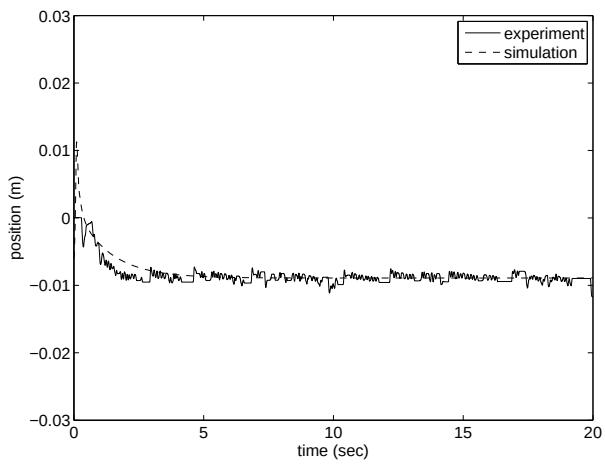

Figure 10. Implementation of the controller based on the dynamic friction model in the experiment (solid line) and in a numerical simulation of the system with initial condition $(x, \theta, \dot{x}, \dot{\theta}) = (0, 0.02 \text{ rad}, 0, 0)$ (dashed line).

We assume that there is a time delay, $\tau > 0$, between when the variables used in the feedback law (13) are measured and when the voltage $V(t)$ is applied. Adding this delay to the model, the applied force in (1) now becomes

$$F(t) = d_1 x(t-\tau) + d_2\theta(t-\tau) + d_3\dot{x}(t-\tau) + d_4\dot{\theta}(t-\tau) - \beta\dot{x}(t), \tag{26}$$

where $d_i = \alpha k_i$.

We wish to find the smallest time $\tau_c > 0$ that makes the upright equilibrium point of this system unstable. Rewriting the model as a first order system and linearizing about the upright equilibrium point yields the system

$$\dot{\mathbf{y}} = A\mathbf{y}(t) + E\mathbf{y}(t-\tau) \tag{27}$$

where $\mathbf{y}$ and A and E depend on which friction model is used. We find the critical time delay, τ_c, by assuming that equation (27) has a solution of the form $\mathbf{y}(t) = \mathbf{v}e^{\lambda t}$, substituting $\mathbf{y}(t)$ back into the equation and solving for the smallest value of τ such that the system has an eigenvalue λ with $Re(\lambda) = 0$.

5.1 Time Delay with the Exponential Friction Model

For the exponential model, $\mathbf{y} = [x, \theta, \dot{x}, \dot{\theta}]$, and A and E in (27) are:

$$A = \begin{pmatrix} 0 & 0 & 1 & 0 \\ 0 & 0 & 0 & 1 \\ 0 & \frac{-3mg}{4M+m} & \frac{-(\beta+\varepsilon+\delta\mu_s(M+m)g)}{4M+m} & 0 \\ 0 & \frac{3(M+m)g}{(4M+m)l} & \frac{3(\beta+\varepsilon+\delta\mu_s(M+m)g)}{(4M+m)l} & 0 \end{pmatrix}, \tag{28}$$

$$E = \begin{pmatrix} 0 & 0 & 0 & 0 \\ 0 & 0 & 0 & 0 \\ \frac{4d_1}{4M+m} & \frac{4d_2}{4M+m} & \frac{4d_3}{4M+m} & \frac{4d_4}{4M+m} \\ \frac{-3d_1}{(4M+m)l} & \frac{-3d_2}{4M+m} & \frac{-3d_3}{4M+m} & \frac{-3d_4}{4M+m} \end{pmatrix}. \tag{29}$$

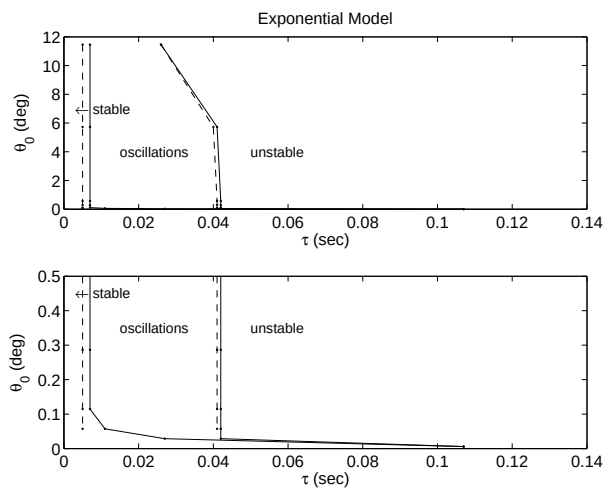

Figure 11. Results of numerical simulations of (1) with the exponential friction model and corresponding feedback gain (23). Dashed lines correspond to using the friction model (8). Solid lines correspond to replacing $\mathrm{sgn}(\dot{x})$ with $\tanh(100\dot{x})$. Initial conditions used are as in (30) for various values θ_0 of the time delay, τ. The bottom graph shows a zoom in of the top graph.

Using the parameters in Tables 1 and 3 and $\delta = 100$, we find that the critical time delay is $\tau_c \approx 0.1069$ seconds.

To study this experimentally, we implemented the feedback control based on the exponential friction model, i.e., (26) with gain given by (23), in our experimental system. The actual time delay of the experimental system is insignificant, however, we can artificially vary it using the computer system which implements the feedback control. We did this and observed that the upright equilibrium point was asymptotically stable until $\tau = 0.01$. For $0.01 < \tau < 0.025$ the experimental system exhibited oscillations about the upright equilibrium point, with amplitude that increased with τ. For $\tau \geq 0.025$, the pendulum fell down. Our initial conditions for the experiment are set manually, by holding the pendulum "close" to the upright position. Thus they are given by

$$x(t) = 0, \theta(t) = \theta_0, \dot{x}(t) = 0, \dot{\theta}(t) = 0, \ -\tau \leq t \leq 0. \tag{30}$$

The range of initial angles that we used was approximately $1 \leq \theta_0 \leq 5$ degrees.

To understand the discrepancy between our theoretical prediction and experimental results, we performed numerical simulations of the full model (1) with the delayed force (26) and exponential friction model (8). The simulations were performed in the Matlab Simulink tool box using the solver `ode23tb`, which is a variable step size solver for stiff differential equations, using initial conditions (30) with $\theta_0 \leq 10$ deg. The results are summarized in the top graph of Figure 11 (dashed lines) with a zoom in shown in the bottom graph. For all initial conditions tested, we found that the equilibrium point was stable for $\tau < 0.005$. With $0.06 < \theta_0 < 6$ degrees, the system exhibited oscillations for $0.005 \leq \tau < 0.041$ and the pendulum fell over for $\tau \geq 0.041$. For $\theta_0 \geq 6$ degrees, the delay value at which the transition from oscillations to instability occurred decreased with increasing θ_0. The numerical integration routine had difficulty dealing with initial conditions smaller than 0.06 degree due to the signum function. Clearly, the simulation results match the experimental observations better than the theoretical prediction based on the linearization of the model with the smooth approximation to the signum function. However, we still have no explanation for the discrepancy between the destabilizing delay predicted by linearization and that observed in the experiment.

To investigate this discrepancy further, we performed simulations using the smooth approximation $\tanh(100\dot{x})$ for $\mathrm{sgn}(\dot{x})$ in (8). The results of these simulations are summarized in the top graph of Figure 11 (solid lines) with a zoom in shown in the bottom graph. For initial conditions with $\theta_0 > 0.1$ degree, these simulations give very similar results to the model with the signum function. For smaller initial conditions, however, the two transition values of the delay increase and finally coalesce. For small enough initial conditions the delay where stability is lost matches the theoretical prediction from the linearization, as it should.

These results lead to two possible explanations for the discrepancy between the theoretical prediction and the experimental observation.

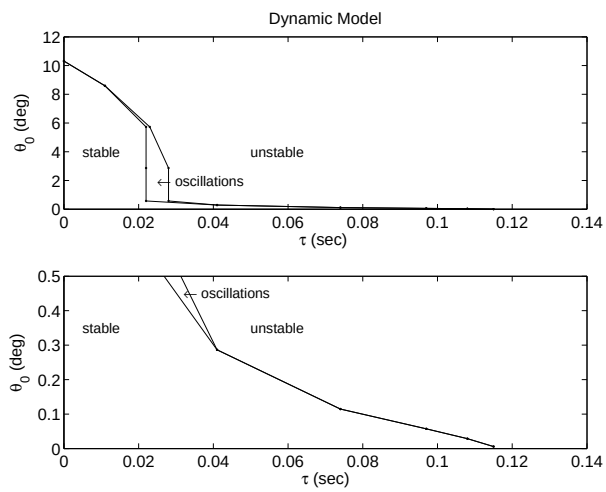

Figure 12. Results of numerical simulations of (1) with the dynamic friction model and corresponding feedback gain. Initial conditions used are as in (30) for various values θ_0 of the time delay, τ. The bottom graph shows a zoom in of the top graph.

The simplest is that while the smooth approximation is good enough to design a controller which will stabilize the system, it is not good enough to use for quantitative predictions of delay induced instability. Alternatively, we note that simulations with the smooth approximation show that when $0.007 < \tau \leq \tau_c$ only for very small initial conditions will the system return to the stable equilibrium point. This situation, where the equilibrium point is asymptotically stable, but only for initial conditions sufficiently close to the point is called *local* asymptotic stability. Of course, local stability is all that is guaranteed by the linear stability analysis. We cannot verify this idea experimentally, since it is impossible to get the pendulum sufficiently close to the equilibrium point. However, we can conclude from both sets of simulations that the *effective* critical delay (i.e. the delay where stability will be lost with experimentally achievable initial conditions) is considerably less than that predicted by the linear stability analysis.

5.2 Time Delay with the Dynamic Friction Model

For the dynamic friction model, $\mathbf{y} = [x, \theta, \dot{x}, \dot{\theta}, z]$, and A and E in (27) are:

$$A = \begin{pmatrix} 0 & 0 & 1 & 0 & 0 \\ 0 & 0 & 0 & 1 & 0 \\ 0 & \frac{-3mg}{4M+m} & \frac{-4(\beta+\sigma_1+\sigma_2)}{4M+m} & 0 & \frac{-4\sigma_0}{4M+m} \\ 0 & \frac{3(M+m)g}{(4M+m)l} & \frac{3(\beta+\sigma_1+\sigma_2)}{(4M+m)l} & 0 & \frac{3\sigma_0}{(4M+m)l} \\ 0 & 0 & 1 & 0 & 0 \end{pmatrix}, \tag{31}$$

$$E = \begin{pmatrix} 0 & 0 & 0 & 0 & 0 \\ 0 & 0 & 0 & 0 & 0 \\ \frac{4d_1}{4M+m} & \frac{4d_2}{4M+m} & \frac{4d_3}{4M+m} & \frac{4d_4}{4M+m} & 0 \\ \frac{-3d_1}{(4M+m)l} & \frac{-3d_2}{4M+m} & \frac{-3d_3}{4M+m} & \frac{-3d_4}{4M+m} & 0 \\ 0 & 0 & 0 & 0 & 0 \end{pmatrix}. \tag{32}$$

Using the parameters in Tables 1–4, we find that the critical time delay is $\tau_c \approx 0.1169$ seconds.

To study this experimentally, we implemented the feedback control based on the dynamic friction model, i.e., (26) with gain given by (25), in our experimental system and varied the time delay as described above. We observed that the upright equilibrium point was asymptotically stable until $\tau = 0.009$. For $0.009 < \tau < 0.023$ the experimental system exhibited oscillations about the upright equilibrium

point, with amplitude that increases with τ. For $\tau > 0.023$, the pendulum fell down.

To understand the discrepancy between our theoretical prediction and experimental results, we performed numerical simulations of the full model (1) with the delayed force (26) and the dynamic friction model (11). The simulations were performed using the same package as for the exponential friction model. The results of these simulations are summarized in top graph of Figure 12 with a zoom in shown in the bottom graph. We find a similar situation to that with the numerical simulations of the exponential model with the smooth approximation to the signum function. For initial conditions with $1 < \theta_0 < 5$ degrees, the *effective* critical delay is 0.022 and for larger initial conditions, the effective critical delay is even smaller. The simulations also show that, for $1 < \theta_0 < 5$ degrees, the system exhibits oscillations for $0.022 \leq \tau < 0.028$ and the pendulum falls down for $\tau > 0.028$. These predictions are in reasonable agreement with the experimental observations. The prediction of the destabilizing delay is not as good as that using the exponential friction model, however the prediction of the delay when the pendulum falls over is better. The simulations for initial conditions with $\theta_0 < 1$ show that the effective critical delay increases as θ_0 decreases, limiting close to the theoretically predicted critical delay as θ_0 goes to zero. This gives an explanation for the discrepancy between the experimental observations and the theoretical prediction of the critical delay. Namely, the equilibrium point is only locally asymptotically stable, and for large delays can only be observed for initial angles smaller than can be achieved experimentally.

6 Conclusions

We have studied a model for an experimental pendulum system where feedback control is used to maintain the pendulum in the upright position. The main focus of our study was how the model for friction between the cart and the track affects the performance of the controller. Previous work used a simple viscous friction model to design the controller. This resulted in small amplitude oscillations when this controller was implemented in the experimental system. We gave a possible explanation of this behaviour by studying the situation when the controller designed using a simple viscous friction model is implemented in a model which incorporates stick slip friction. We considered two stick slip friction models: exponential and dynamic. We showed that the controller may fail (the equilibrium point is not linearly stable) or have bad performance (the equilibrium point is linearly stable, but has a small basin of attraction). The results depended on the model of stick slip friction used. With both stick slip friction models, numerical simulations revealed stable, small amplitude oscillations that are very similar to those observed in the experiment.

We then used the stick slip friction models to design new controllers for the system and showed, analytically, numerically and experimentally, that our new controllers stabilize the equilibrium point and give good performance in the sense that the equilibrium point has a large basin of attraction. Controllers designed using either stick slip model displayed similar performance. The dynamic friction model possesses an uncontrollable state which made controller design more complicated.

With a new controller designed using a stick slip friction model, the system is stable, but still has some noise. By running a frequency analysis on the experiment, we determined that the most likely source of this noise was the sensors. The angle sensor has a resolution of 0.08789 degrees and the position sensor an accuracy of 0.00454 cm. Any changes in the angle or position smaller than the these resolutions will not be detected by the sensor and may cause small jumps in the inputs to the controller. These jumps display as noise and are most apparent when the system is nearly stationary. When the experimental data was studied further, it seems that the angle sensor is the main problem. This can be seen in Figure 13. Part (a) is the experimental data for the angle corresponding to the position data of Figure 9. Part (b) is a magnification of one part of the data, clearly showing the jumps in angle measurement. We expect that the controlled system performance could be reduced by using an angle sensor with better resolution.

Finally, we studied the effect of time delay in the feedback control. We found that the exponential friction model was slightly more robust to time delay (critical delay of 0.01 sec vs 0.009 sec). Linear stability analysis of the model gave a poor prediction of the critical time delay. A much better prediction was obtained from numerical simulations of the full nonlinear model. The reason for this is that for a large range of delay values, the upright equilibrium point is locally stable and only initial conditions starting very close to the equilibrium point achieve stability. Other initial conditions either result in oscillations or the pendulum falling down. Since it is difficult to experimentally achieve initial conditions very close to the equilibrium point, the effective critical delay is larger than that predicted by linear stability analysis.

The main conclusion of our work is that, when choosing a model to be used in designing a controller, it is critical not only to include friction in the model but to include the correct type of friction and to estimate the parameters as accurately as possible. For systems with stick slip friction, we found that both the models of [9] and [10] are adequate. Controllers based on either model stabilize the pendulum

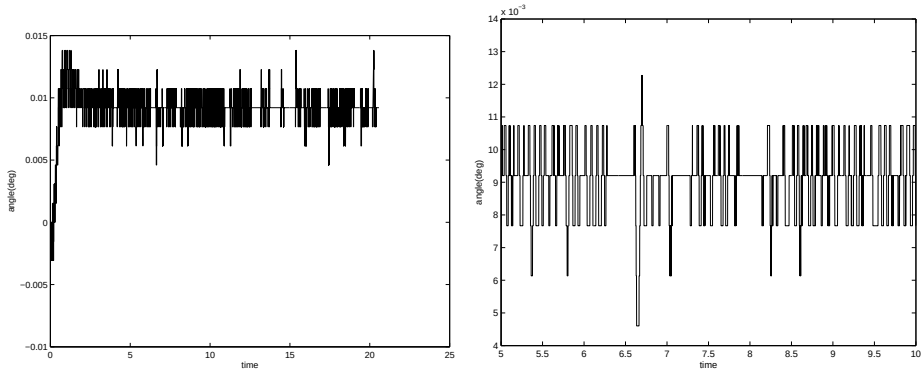

(a) (b)

Figure 13. (a) Angle data for the experiment of Figure 9. (b) Magnification, showing jumps due to angle sensor resolution.

in the upright position. Both models have drawbacks. It is more difficult to calculate the controller for the model of [10]. However, numerical simulations of using the model of [9] are difficult, due to the discontinuities in the model.

Acknowledgements

This research was supported by the Natural Sciences and Engineering Research Council (NSERC) of Canada, through the Discovery Grants and Undergraduate Summer Research Awards programs.

7 Estimation of Friction Parameters

To find values for the various parameters in our friction model, we need to measure the friction force in our physical system. We will assume that the friction is only due to the interaction between the cart and the track. Thus, we will use the physical system without the pendulum to experimentally measure the friction force. Using Newton's law, the equation of motion of the isolated cart is:

$$M\ddot{x} = \alpha V(t) - \beta\dot{x} + F_{\text{fric}}, \tag{33}$$

where $\alpha V(t) - \beta\dot{x}$ is the net force applied to the cart by the motor driving the cart, as described in section 1, and F_{fric} is the friction force.

7.1 Estimating the Coefficients of Coulomb and Viscous Friction

When the cart is in motion, it has two kinds of friction acting on it: viscous and Coulomb (sliding) friction. Recalling the discussion of section 2, the the friction force when the cart is in motion is given by:

$$F_{\text{fric}} = -\mu_c F_N \operatorname{sgn}(\dot{x}) - \varepsilon\dot{x}. \tag{34}$$

In our experiments, the cart only moves forward, thus $\operatorname{sgn}(\dot{x}) = 1$. Further, since the pendulum is removed from the cart and the cart moves horizontally, $F_N = Mg$. Thus the equation becomes

$$F_{\text{fric}} = -\mu_c Mg - \varepsilon\dot{x}. \tag{35}$$

If we let the cart run forward long enough at a constant voltage, it will stop accelerating and reach a constant velocity. Thus $\ddot{x} = 0$ and

$$\begin{aligned} \alpha V - \beta \dot{x} &= -F_{\text{fric}} \\ &= \mu_c M g + \varepsilon \dot{x} \end{aligned} \tag{36}$$

Given two values for the constant applied voltage, V, and the constant final velocity, $\dot{x}$, equation (36) can be used to calculate the Coulomb and viscous friction coefficients, μ_c and ε. To get a better estimate, we ran the experiment for 10 different voltages. A typical run is shown by the solid line Figure 4(b). We then calculated the corresponding final velocity for each voltage, as shown in Table 5, and used the results pairwise to estimate μ_c and ε. These estimates of μ_c and ε were averaged to obtain the values $\mu_c = 0.04287$, $\varepsilon = 2.3156$.

Table 5. Experiment with Constant Applied Voltage

Applied Voltage	Final Velocities			Average
0.8	0.1039	0.137	0.1014	0.1030
1.0	0.1379	0.1319	0.1374	0.1357
1.2	0.1672	0.1701	-	0.1686
1.4	0.2113	0.2105	0.2090	0.2103
1.6	0.2382	0.2297	-	0.2339
1.8	0.2848	0.2708	-	0.2778
2.0	0.2992	0.2983	0.3000	0.2992
2.2	0.3419	0.3445	0.3328	0.3397
2.4	0.3804	0.3832	-	0.3818
2.6	0.4100	-	-	0.4100

7.2 Estimating the Coefficient of Static Friction

Static friction refers to the friction needed to be overcome for the cart to start moving. It is very difficult to accurately measure the value of the static friction coefficient, however, Armstrong-Hélouvry [12] have outlined a procedure which we follow here. From the static friction model (5), at the instant the cart starts to move, the magnitude of the static friction force is equal to that of the applied force. For our experimental setup with the pendulum detached from the cart, this leads to $F_{\text{static}} = F_{\text{applied}}$ or

$$\mu_s M g = \alpha V_s \tag{37}$$

where V_s is the voltage in the motor at the moment the cart starts to move. To measure this voltage, we used a voltage ramp, i.e. the voltage in the cart was is gradually increased until the cart moved. The voltage and position of the cart are recorded and the voltage needed to get the cart moving without stopping again is estimated from this data. Ten runs were done and the estimated voltages are shown in Table 6. The average of these values is 0.38697. Equation (37) with the values of the parameters from Table 1 yields $\mu_s = .8328$.

Table 6. Voltages for Measurement of Static Friction

Number	Voltage
1	0.3655
2	0.36795
3	0.4166
4	0.40085
5	0.3464
6	0.3725
7	0.3632
8	0.40465
9	0.44765
10	0.3844

REFERENCES

[1] Morris, K., and Juang, J., 1993. "Dissipative controller design for second-order dynamic systems". In Control of Flexible Structures, K. Morris, ed., AMS, pp. 71–90.

[2] Olsson, H., and Astrom, K., 2001. "Friction generated limit cycles". *IEEE Trans. Contr. Syst. Technol.*, **9**(4), pp. 629–636.

[3] Hirschorn, R., and Miller, G., 1999. "Control of nonlinear systems with friction". *IEEE Trans. Contr. Syst. Technol.*, **7**(5), pp. 588–595.

[4] Kollár, L., Stépán, G., and Hogan, S., 2000. "Sampling delay and backlash in balancing systems". *Periodica Polytechnica Ser. Mech. Eng.*, **44**(1), pp. 77–84.

[5] Bugeja, M., 2003. "Non-linear swing-up and stabilizing control fo an inverted pendulum system". In Proceedings of the IEEE Region 8 EUROCON 2003: Computer as a Tool, B. Zajc and M. Tkalčič, eds., Vol. 2, IEEE, pp. 437–441.

[6] Yoshida, K., 1999. "Swing-up control of an inverted pendulum by energe-based methods". In Proceedings of the 1999 American Control Conference, Vol. 6, pp. 4045–4047.

[7] Landry, M., Campbell, S., Morris, K., and Aguilar, C., 2005. "Dynamics of an inverted pendulum with delayed feedback control". *siamjads*, **4**(2), pp. 333–351.

[8] Morris, K., 2001. *An Introduction to Feedback Controller Design*. Harcourt/Academic Press.

[9] Hauschild, J., 2003. "Control of a flexible link robotic manipulator in zero gravity conditions". Tech. rep., University of Waterloo.

[10] Canudas de Wit, C., and Lipschinsky, P., 1995. "A new model for control systems with friction". *IEEE Transactions on Automatic Control*, **40**(3).

[11] Golubitsky, M., Stewart, I., and Schaeffer, D., 1988. *Singularities and Groups in Bifurcation Theory*, Vol. 2. Springer Verlag, New York.

[12] Armstrong-Hélouvry, B., 1991. *Control of Machines with Friction*. Kluwer, Boston.